

Review

Structural Studies of Bacteriophage $\Phi 6$ and Its Transformations during Its Life Cycle

J. Bernard Heymann ^{1,2} 

¹ National Institute of Arthritis and Musculoskeletal and Skin Diseases, National Institutes of Health, 50 South Dr., Bethesda, MD 20892, USA; heymannb@mail.nih.gov; Tel.: +1-301-846-6924

² National Cryo-EM Program, Cancer Research Technology Program, Frederick National Laboratory for Cancer Research, Leidos Biomedical Research, Inc., Frederick, MD 21701, USA

Abstract: From the first isolation of the cystovirus bacteriophage $\Phi 6$ from *Pseudomonas syringae* 50 years ago, we have progressed to a better understanding of the structure and transformations of many parts of the virion. The three-layered virion, encapsulating the tripartite double-stranded RNA (dsRNA) genome, breaches the cell envelope upon infection, generates its own transcripts, and coopts the bacterial machinery to produce its proteins. The generation of a new virion starts with a procapsid with a contracted shape, followed by the packaging of single-stranded RNA segments with concurrent expansion of the capsid, and finally replication to reconstitute the dsRNA genome. The outer two layers are then added, and the fully formed virion released by cell lysis. Most of the procapsid structure, composed of the proteins P1, P2, P4, and P7 is now known, as well as its transformations to the mature, packaged nucleocapsid. The outer two layers are less well-studied. One additional study investigated the binding of the host protein YajQ to the infecting nucleocapsid, where it enhances the transcription of the large RNA segment that codes for the capsid proteins. Finally, I relate the structural aspects of bacteriophage $\Phi 6$ to those of other dsRNA viruses, noting the similarities and differences.

Keywords: *Cystoviridae*; cryoEM; dsRNA; ssRNA; RNA-dependent RNA polymerase; virus capsid; virus envelope; virus infection



Citation: Heymann, J.B. Structural Studies of Bacteriophage $\Phi 6$ and Its Transformations during Its Life Cycle. *Viruses* **2023**, *15*, 2404. <https://doi.org/10.3390/v15122404>

Academic Editor: Paul Gottlieb

Received: 24 October 2023

Revised: 1 December 2023

Accepted: 4 December 2023

Published: 11 December 2023



Copyright: © 2023 by the author. Licensee MDPI, Basel, Switzerland. This article is an open access article distributed under the terms and conditions of the Creative Commons Attribution (CC BY) license (<https://creativecommons.org/licenses/by/4.0/>).

1. Significance of Bacteriophage $\Phi 6$

The members of the *Cystoviridae* are the only known double-stranded RNA (dsRNA) bacteriophages, with bacteriophage $\Phi 6$ being the first isolated and the type species of the family [1]. Additional members of the family are being added [2], including bacteriophages $\Phi 8$, $\Phi 12$, and $\Phi 13$, as mentioned in this review. They represent counterparts to the dsRNA viruses, infecting eucaryotes and offer simpler systems for studies of structure and life cycle. These involve questions such as how the genome is encapsidated in the protective virus shells [3] and the roles of the component proteins in the propagation of the virus. Such insights may lead to the development of antivirals and treatments for managing pathogenic viruses [4]. In addition, the presence of dsRNA is typically a sign of viral infection [5].

The host of bacteriophage $\Phi 6$, *Pseudomonas syringae* (previously known as *P. phaseolicola*), is a plant pathogen of commercial importance in agriculture. One potential use for such a phage is therefore in controlling bacterial infections in plants [6,7].

In recent years, bacteriophage $\Phi 6$ has been used as a surrogate for enveloped viruses such as SARS-CoV-2 [4]. Used with care to acknowledge differences [8], it can be a valuable tool to understand environmental factors associated with viral infectivity without undue exposure to a dangerous virus.

2. Life Cycle of Bacteriophage $\Phi 6$

The $\Phi 6$ virion is composed of multiple layers, with the P1 protein forming an icosahedral capsid shell enclosing the dsRNA genome, in turn surrounded by an intermediate

shell composed of proteins P4 and P8, and finally covered by an outer protein-lipid shell or envelope (Figure 1). The genome itself is divided into three parts: small (S), medium (M), and large (L) segments of dsRNA (the ssRNA transcripts are denoted as *s*, *m*, and *l* in lowercase. See [9]. for examples). The segments code for proteins at different stages of the life cycle (Figure 2) [10]. Upon infection, virions first bind to the host pili [1], requiring the protein P3 anchored onto P6 [11]. The pili then retract, and the virions fuse with the outer membrane mediated by the P6 protein [11]. The lysin (protein P5) degrades the peptidoglycan layer [12,13], allowing viral particle access to the inner membrane, which can then be traversed in an energy-dependent manner [14]. The P8 layer is subsequently stripped off and degraded [14]. What remains is the nucleocapsid, decorated with the P4 protein on the outside, producing ssRNA transcripts. A host protein, YajQ, binds to the outside of the nucleocapsid to enhance the transcription of the L segment [15]. The transcripts from all three segments are exported and translated into different viral proteins by the host machinery.

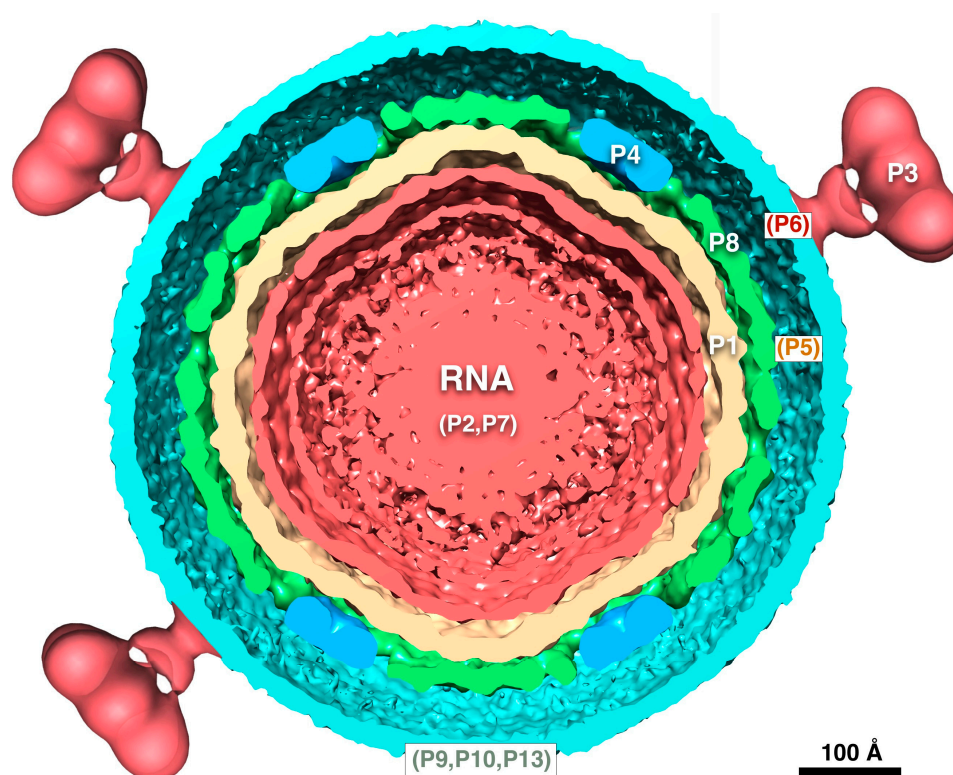


Figure 1. The bacteriophage $\Phi 6$ virion. The dsRNA is packaged within an icosahedral P1 shell together with proteins P2 and P7. Proteins P4 and P8 form an intermediate layer, surrounded by the envelope featuring the spike protein P3. Proteins in brackets have only approximate locations within the virion. (Map based on EMDB 1301 [16] and the spike from $\Phi 12$ [17]).

The four translation products of the *l* segment, P1, P2, P4, and P7, assemble into procapsids [18,19]. The three ssRNA segments are then sequentially packaged into the capsid [20], with concurrent expansion. Minus strand synthesis (replication) follows the completion of the packaging of the *l* segment [9]. The P8 layer is then assembled onto the new nucleocapsids [14]. The non-structural protein, P12, is required by P9 to form the proteolipid envelope, incorporating proteins P3, P6, P10, and P13 [21]. The proteins P5 and P10 cause cell lysis and the release of progeny virions [12,22].

The quantitation of the copy number of every protein is important for understanding the assembly and transformations of the virion and its sub-particles during the life cycle [23]. In the following section, I will cover not only the structure but also the copy numbers of the various proteins and how that relates to function. There will also be references to the

structures of related viruses, such as $\Phi 8$ and $\Phi 12$. These show some sequence similarity but with very similar genomic organization protein structures [2].

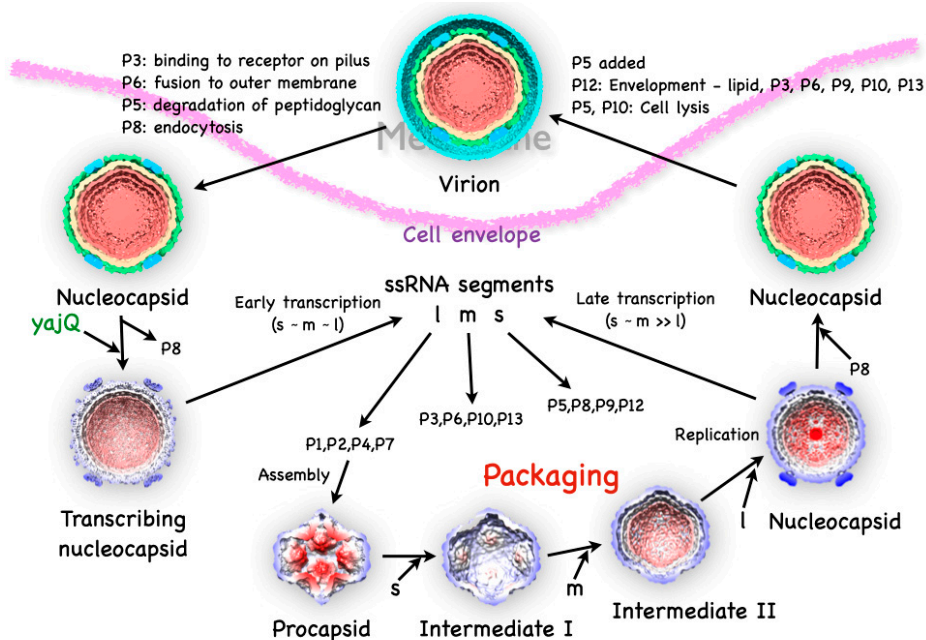


Figure 2. The bacteriophage $\Phi 6$ life cycle in structures. The virion has three layers surrounding the tripartite dsRNA genome (red): the capsid (beige), the intermediate layer (blue and green), and the proteolipid envelope (cyan). Infection starts when the P3 spike binds to the pilus receptor. The envelope then fuses with the outer membrane, degrades the peptidoglycan layer (P5), and enters, mediated by P8. After P8 disassembles, the host factor YajQ binds to facilitate the transcription of the l segment, so that it is expressed at about the same levels as the s and m segments. The l segment codes for the four proteins assembled into the initial product, the procapsid. The ssRNA segments are then packaged in sequence with corresponding expansion of the capsid shell. Once all the segments are packaged, replication completes the production of the dsRNA genome. The P8 shell is assembled, the envelope added, and the new virion released through cell lysis.

3. The Initial Assembly Product, Procapsid

The procapsid (also called the polymerase complex) consists of four proteins [18]: P1, which makes up the icosahedral shell; P2, the RNA-dependent RNA polymerase (RdRP) [24]; P4, the packaging motor [25,26]; and P7, an assembly and packaging enhancer [27,28]. Early attempts to crystallize the procapsid failed, opening the way for studies by electron microscopy. As will be discussed later, the procapsid is in a metastable state, and the P4 protein is a hexamer in a symmetry-mismatch position weakly bound to the P1 shell. These features may not be conducive to stable crystal contacts and required imaging by electron microscopy of fresh samples soon after preparation.

3.1. The P1 Shell

The main part of the procapsid consists of an icosahedral shell formed by the 85 kDa P1 protein [29]. Early cryoEM reconstructions revealed a compact particle with invaginated five-fold vertices, giving it a star-like appearance (Figure 3A) [30–35].

The stoichiometry of the virion indicated that there are 120 copies of the P1 protein per particle [23], which means there are two copies per asymmetric unit, similar to other dsRNA viruses (Figure 3C) [30,36]. Better cryoEM reconstructions allowed for the discernment of structural details of the two copies [31] and eventually to near-atomic detail [37]. The architecture is very similar in the related bacteriophage $\Phi 8$ [16].

While the whole procapsid could not be crystallized, a pentamer of P1 in the presence of P7 was solved (Figure 3B) [37]. Similarly, a pentamer of the P1 from $\Phi 8$ was also solved

by X-ray crystallography [38]. The pentamer forms the invaginated five-fold vertices, and the subunits are designated as P1_A (blue in Figure 3C). The other subunits are designated as P1_B, connecting the two-fold and three-fold axes (red/orange/yellow in Figure 3C). P1_A and P1_B have identical folds with only minor differences in conformation to adapt to their different positions in the capsid (an example of “quasi-equivalence” of the subunits of the capsid [39]) [37].

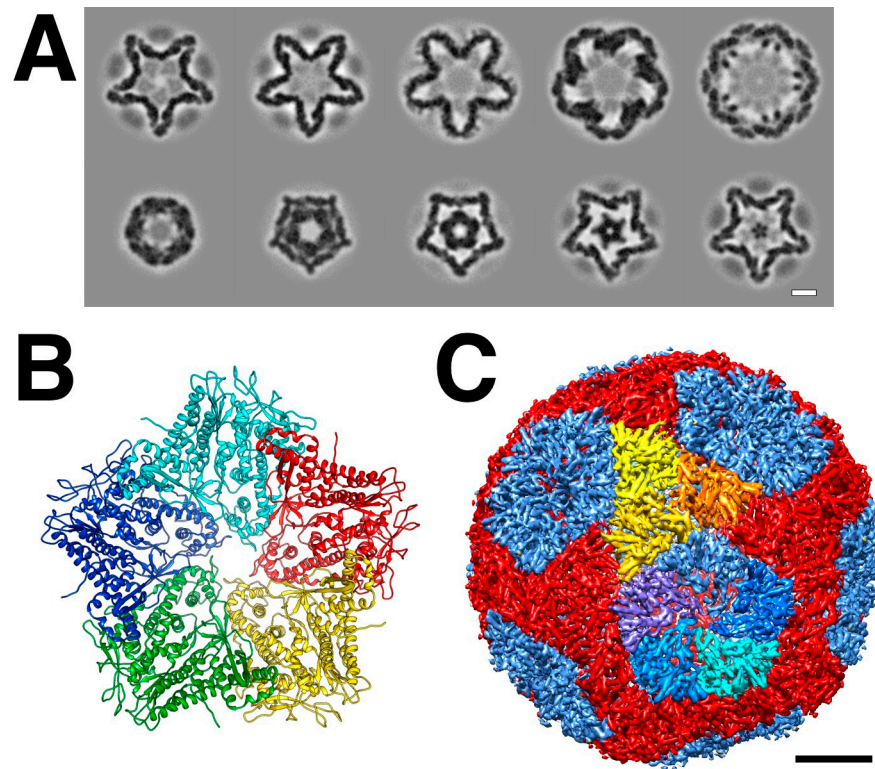


Figure 3. The procapsid shell. (A) Sections through a procapsid showing the invaginated five-fold vertices of the P1 shell. The diffuse densities are the minor procapsid proteins. (EMDB: 1501) [32] (B) The pentamer of P1 solved by X-ray crystallography. (PDB: 4K7H) [37] (C) Distinction of the P1_A (blues) and P1_B (red, orange, yellow) subunits in the procapsid. Scale bars: 100 Å.

3.2. The Packaging Motor, Protein P4

The 35 kDa protein P4 was identified as an NTPase required for the packaging of positive ssRNA strands into the procapsid [25,26]. The P4 protein forms a hexamer [40,41] that sits in the five-fold invagination in the procapsid with an obvious symmetry mismatch [42]. Both in virions, as well as recombinant and assembled procapsids, about 60–70 P4 monomers per particle were reported, close to the expected 72 (12 hexamers) [43]. In bacteriophage Φ 8 nucleocapsids, the average occupancy of P4 on the five-fold vertices were found to be ~60 [44]. However, isolated Φ 6 procapsids in other studies consistently had lower copy numbers [33–35]. Increased ionic strength, heat, and acidic conditions lead to P4 dissociation and procapsid expansion [33,45,46]. The interaction between P4 and P1 is therefore rather weak, perhaps tuned to intracellular conditions differing significantly from those in isolates.

Both available high-resolution procapsid reconstructions have very low P4 density [37,47], precluding assessing its association with the P1 shell. It is likely that the same interaction is maintained in the nucleocapsid, where we have several reconstructions. An asymmetric reconstruction of the five-fold vertex shows the P4 hexamer on top of the P1 shell and surrounded by the P8 layer (Figure 4A,C) [48]. Because of the symmetry mismatch, only some of the protrusions from the hexamer are expected to interact with P1. In Figure 4B, the thresholding of the isosurface was adjusted to show four possible

connections. Sun et al. [48] identified a density not attributed to the P1 shell but consistent with the C-terminal tail of P4 (Figure 4D). The C-terminal 13 residues were previously shown to be important for procapsid assembly [49]. This tail extends over both the P1_A and P1_B subunits. The density is strong enough to suggest that five of the six P4 C-termini bind to the P4 shell. In procapsids, P4 is often shifted slightly from the five-fold axis [33], suggesting that some of its C-terminal tethers may be less tightly bound.

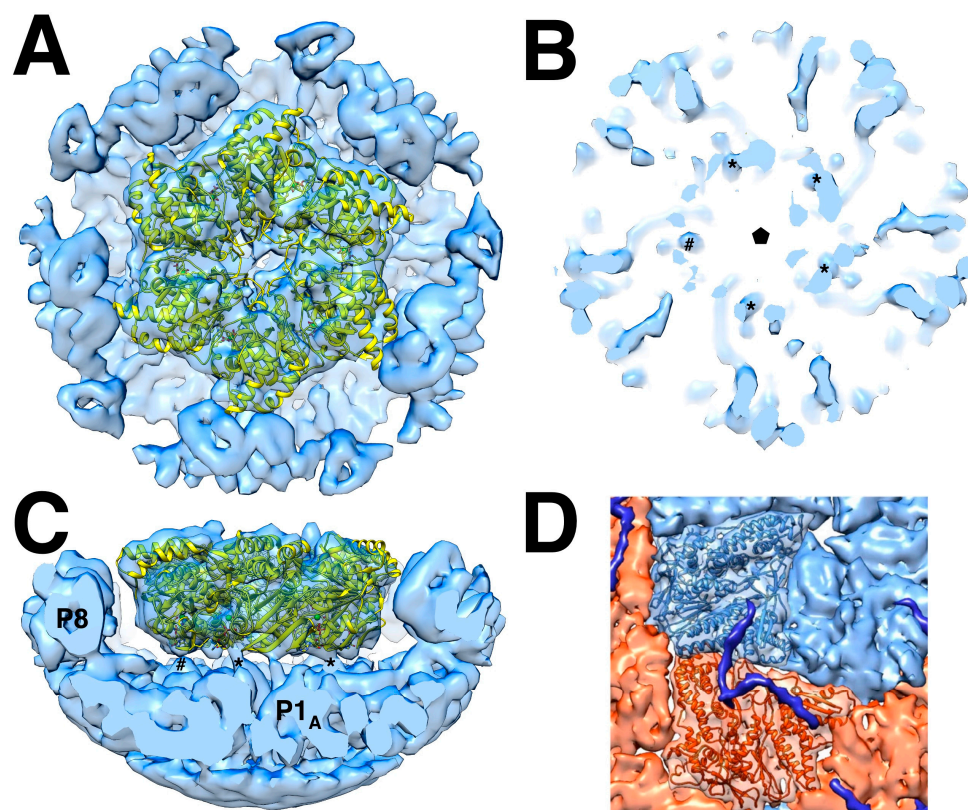


Figure 4. The packaging motor, P4: (A) The P4 X-ray crystal structure (PDB: 5MUU) fitted into the density of an asymmetric reconstruction of the five-fold vertex of the nucleocapsid (EMDB: 3573), surrounded by the P8 layer. (B) A section through the reconstruction at the contact plane reveals four possible connections (*), with the fifth (#) not quite forming a connection. (C) Side view showing the connections between P4 and the capsid shell below. (D) The C-terminal tail of P4 (blue) traverses the surfaces of P1_A (light blue) and P1_B (red) [48].

3.3. The RNA-Dependent RNA Polymerase, Protein P2

The whole $\Phi 6$ procapsid was functionally referred to as the polymerase complex because of its activity in transcription and replication [50,51]. The 75 kDa protein P2 was identified as the actual polymerase responsible for both replication and transcription [24], and its structure was solved by X-ray crystallography [52].

The polymerase is self-priming, with an emphasis on the first two nucleotides at the 3' of the ssRNA template, fitting into a pocket of the C-terminal domain [52,53]. It can replicate a variety of ssRNA and is stimulated by manganese (II) (Mn^{2+}) [24]. Mn^{2+} appears to lessen the specificity of the polymerase for the 3' terminal sequence [54] by decreasing stability [55], suggesting a mechanism for regulation of its activity. Mn^{2+} consistently enhances activity of polymerases from the related bacteriophages $\Phi 6$, $\Phi 8$, and $\Phi 13$, but with different magnitudes [56], reflecting subtle variations in structure. Self-priming is dependent on the presence of the C-terminal domain linked through residues 601–614 [53]. Mn^{2+} destabilizes the interface of the C-terminal domain to allow for permissive elongation [57]. An amino acid substitution in the Mn^{2+} binding site (E491Q) stabilizes the C-terminal domain, desensitizing it to the stimulatory effect of Mn^{2+} [55]. This becomes

more important in the context of the infection cycle, where $\Phi 6$ developed a mechanism for controlling the production of the *l* transcript by exploiting the host protein, YajQ (see Section 6) [58].

In the early cryoEM reconstructions of the procapsid, P1 and P4 were readily assigned to densities [42], but the locations of both P2 and P7 were not evident. The P2 protein was only located when it was noticed that there is a persistent density on the 3-fold axis inside the procapsid (Figure 5A–C) [32]. Because it exists as a monomer, there is a symmetry mismatch and its density in the cryoEM map is reduced, explaining why it was originally missed. An asymmetric cryoEM reconstruction of the location of P2 on the three-fold axis yielded a map that provided the proper orientation of the molecule (Figure 5D,E) [47]. Specific interactions with P1 in the palm and finger domains were confirmed by mutational analysis [59].

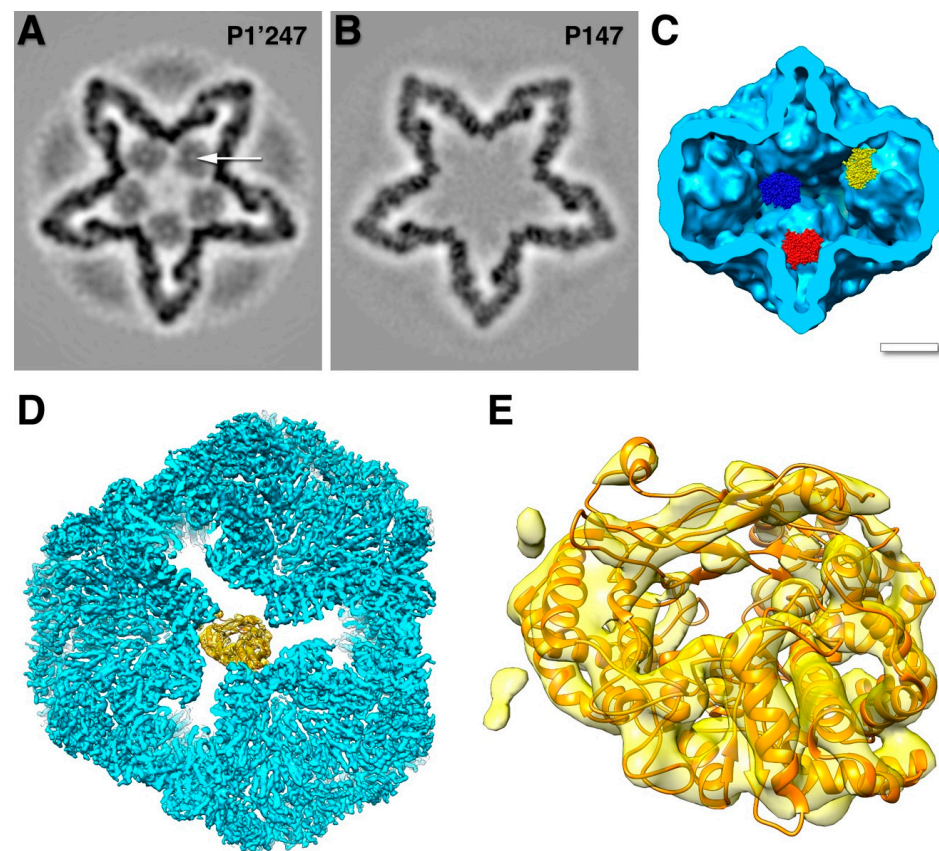


Figure 5. The location of the polymerase in the procapsid. (A) Section through a reconstruction of the procapsid showing the location of the polymerase (arrow). (EMDB: 1501) (B) Section through a reconstruction of a procapsid lacking the polymerase. (EMDB: 1502) (C) Isosurface rendering of a cut through the P1 shell of the procapsid with three polymerase atomic models arranged in the locations indicated in (A) [32]. Scale bar: 100 Å. (D) The polymerase (yellow) within the P1 shell (blue) viewed down a three-fold axis. (EMDB: 3185) (E) Fit of the polymerase crystal structure within the reconstructed density within the context of the P1 shell (EMDB: 3186; PDB: 5FJ6) [47].

Knowing where P2 is located, it can be identified in cryo-electron tomograms of individual procapsids, allowing quantitation by counting [33]. The average occupancy was found to be about 8 out of the 20 possible sites with a distribution that indicates random incorporation during procapsid assembly. This agrees with dose-dependent incorporation during *in vitro* assembly of procapsids [43,59].

3.4. The Packaging Enhancer, Protein P7

The 17 kDa protein P7 enhances assembly of the procapsid and packaging but is not essential in either function [27,28,43,60]. The location of P7 in the procapsid was shrouded in mystery for a time. The only known structure is the N-terminal part of the homologous protein in bacteriophage $\Phi 12$ (Figure 6B) [61]. Because it was solved as a dimer, the initial assumption was that it would be a dimer in the procapsid. It was reported as such a dimer within the intermediate layer, outside the P1 shell [62]. Neutron scattering could only provide a rough radius for both P2 and P7, with P7 possibly located either inside or outside the capsid [63]. Earlier reconstructions of procapsids with and without P7 did not produce any meaningful results [32,42]. With better data and higher resolution maps, P7 was eventually located inside P147 procapsids on the sides of the invaginated five-fold vertices (Figure 6A) [34,35]. The density suggests an orientation of P7 based on the partial structure from $\Phi 12$ (Figure 6C).

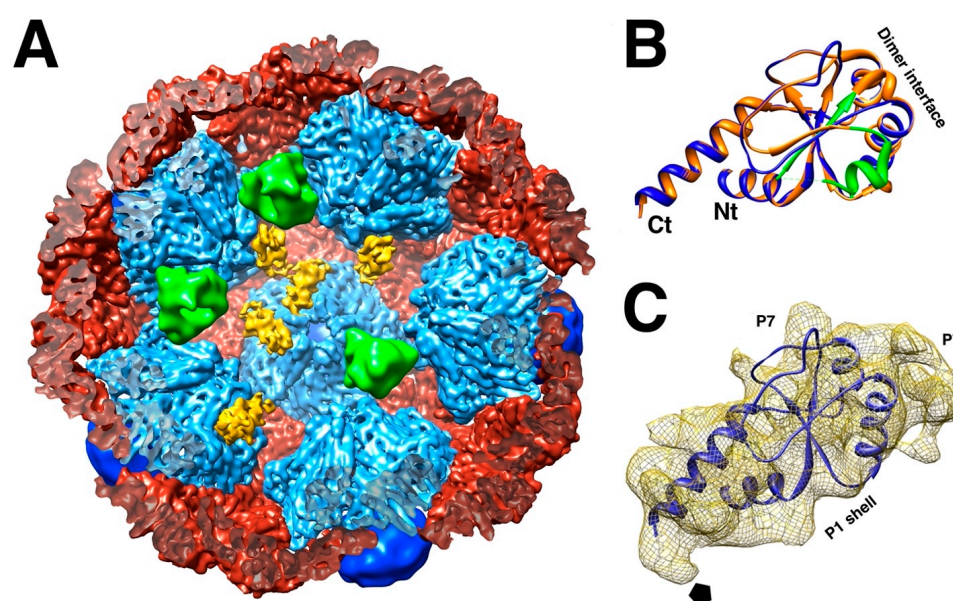


Figure 6. The location of P7. (A) Each P7 monomer (yellow) is bound to the interface between two P1_A subunits (light blue), but only at some locations around the five-fold axis. Polymerase monomers (green) are located at other sites that overlap with the P7 sites. The P1_B subunits (red) and P4 hexamers (dark blue) complete the procapsid. (EMDB: 2341) (B) Homology model of the $\Phi 6$ P7 based on the crystal structure of the $\Phi 12$ P7 protein N-terminal fragment. The dimer interface in the crystal is indicated. (C) One P7 density with a fit of the homology model. Also indicated are the interface to the P1 shell and the interfaces to two potential P7 neighbors around the three-fold axis. The pentagon denotes the five-fold axis [35].

These sites overlap with the location of P2, indicating that the substoichiometric amounts are the result of competitive binding [35]. In assembled procapsids with a large excess of P7, ~60 copies of P7 incorporate into each particle, and the inclusion of P2 is suppressed [43]. However, at about a stoichiometric ratio, the copy number was only ~45 for P7 and 11 for P2 [43], closer to the numbers for recombinant procapsids. From these findings, the expected maximum copy numbers are ~30 for P7 and ~10 for P2, with any excess attributed to non-binding inclusion in *in vitro* assembled particles. Both these proteins appear to be functional in substoichiometric amounts.

3.5. Procapsid Assembly

As is common for many other virus capsids, the procapsids of $\Phi 6$ readily assemble from recombinant constructs *in vivo* or purified proteins *in vitro*. The simplest procapsid obtained is P14 from proteins P1 and P4, while P1 alone or with P7 yields unstable particles

in cells that are fragile to isolation [19]. P1 can form a pentamer in the presence of P7, although P7 was not detected in crystals [37]. The bacteriophage $\Phi 8$ P1 structure was solved as a pentamer without any other proteins [38]. A minimal first product is likely a pentamer of P1_A with P4. The C-terminal tail of P4 extends beyond the P1_A to P1_B [48], suggesting that it could stabilize the addition of P1_B subunits to the pentamer.

Both P2 and P7 accelerate procapsid assembly [59,60]. P2 incorporates in a dose-dependent manner [59], consistent with the random placement at the 20 binding sites [33]. If P2 and P7 are not in the mixture before assembly, they are excluded if added afterward, consistent with their internal location [43]. P2 binds between three invaginated five-fold vertices (Figure 4D) [47] while P7 covers an interface between P1_A subunits (Figure 5A) [35]. The presence of all three accessory proteins, therefore, aids in the efficient production of the P1 shell and acts as the scaffolding commonly observed in other viruses [64].

The sequence of assembly events is uncertain beyond the initial pentamer, likely with a P4 hexamer and 2–3 copies of P7. The potential next step is the addition of P1_B subunits with the involvement of the P4 C-terminal tail. Conceptually, the P1₁₀P4P7_{2–3} units could then come together to form the icosahedral shell with P2 binding between some neighboring P1_A pentamers.

4. Packaging of ssRNA Segments and Capsid Expansion

The packaging of plus-strand RNA in the cystoviruses differ from their eucaryotic counterparts [3]. Cystoviruses package in typical bacteriophage style by insertion into a preformed procapsid driven by a motor protein. Instead, in the *Reoviridae*, the ssRNA first assembles into a particle serving as the nucleating core for the assembly of the capsid shell [65].

From the early cryoEM work on $\Phi 6$, it was clear that the procapsid expands to assume its mature form in the nucleocapsid [30]. The internal volume increases by ~2.5 fold to accommodate the full dsRNA genome [31,45]. Concurrent with expansion, the genomic ssRNA segments package in a strict order, with the s segment first, followed by m and l [20]. The specificity is dependent on conditions with higher magnesium (>4 mM) and phosphate (>1.5 mM) concentrations, rendering the packaging non-specific. Once the l segment is packaged, the polymerase replicates the segments to produce the dsRNA genome [9].

The sequential order of packaging indicates that there should be two expansion intermediates, but only one was identified in the original structural study [30]. In a study where nucleocapsids lost their dsRNA, two partially contracted P1 shells were reconstructed [45]. These were interpreted as lower energy forms of the P1 shell, with the more contracted one indistinguishable from the expanded procapsid and denoted intermediate 1. The intermediate 2 map was constructed from a significant number of particle images indicating it as a clear state. Intermediate 1 is readily obtained by exposing the procapsid to mild heat, acid, or ionic strength conditions [45,46], indicating that the first expansion energy barrier is relatively low (Figure 7). The presence of a 10 × excess of P2 in assembled procapsids appears to prevent expansion [59]. This suggests that the binding of P2 between the invaginated five-fold vertices is strong enough to stabilize the procapsid. On expansion to intermediate 1, P2 is not apparently associated with the P1 shell anymore [45]. The ease with which intermediate 1 is obtained means that it is the more stable conformation of the P1 shell (Figure 7). Presumably, the packaging of the s segment is enough to trigger the first expansion event. The low efficiency of packaging [66] impeded efforts to observe the entry of the s segment by cryoEM.

The current understanding is that the procapsid exists in a metastable state that is easily triggered to expand to intermediate 1, either by acid, heat, or salt, and potentially by the packaging of the s segment generating some pressure inside the procapsid (Figure 7) [45]. The packaging of the m and l segments then increases the pressure on the P1 shell, with it reaching the fully mature state and pressurized state after replication. In reconstructions of the nucleocapsid, the regions around the 5-fold vertices are still flexible, indicating that they do not reach the level of stability of the rest of the capsid.

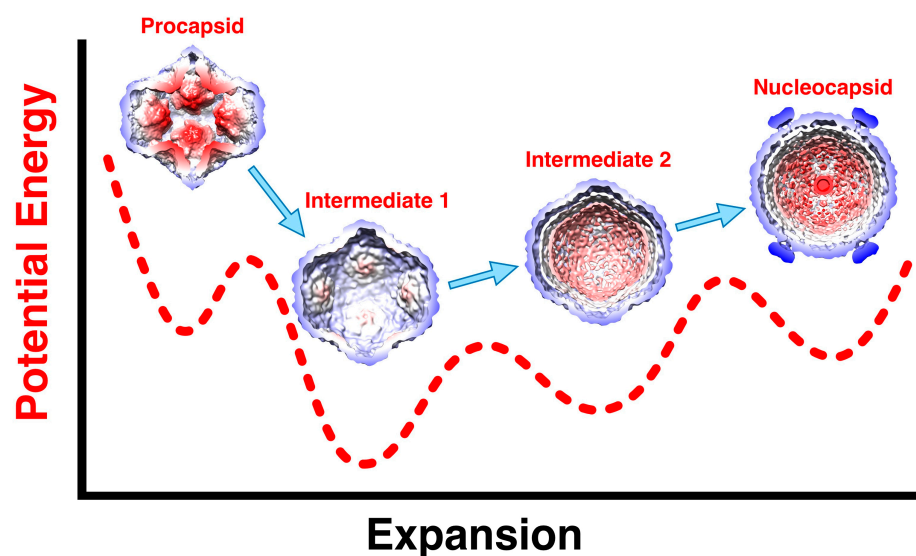


Figure 7. The transformations of the P1 shell on maturation with the dashed curve showing a conceptual energy profile along the expansion coordinate. The procapsid readily converts to the first expansion intermediate by various triggering events such as heat, acid, salt, or the packaging of the s segment. Packaging the m segment then leads to further slight expansion to the second intermediate, followed by packaging the l segment. Only then is the genome replicated to produce the full dsRNA complement.

The demonstration that only one P4 hexamer per procapsid is necessary for packaging followed by minus-strand synthesis (replication) led to the proposal that there is a special vertex different from the others [67]. One possible consequence of such a special vertex is that one would expect there to be a correlation between the locations of P4 hexamer on the outside and the polymerase on the inside. No such correlation was found in a tomographic study of procapsids where individual proteins were counted [33]. It was concluded that such a special vertex is unlikely.

5. Completing the Virion

5.1. dsRNA Packaging of the Nucleocapsid

Remarkably, the dsRNA genome packages in a few configurations amenable to reconstruction such that the helical strands are clear (Figure 8A,B) [68]. In the cytoviruses, defined conformations of the dsRNA have also been found [69,70]. This means that the icosahedral capsids of the dsRNA viruses form very specific interactions with the genome. This is despite the current understanding that the packaging mechanisms are different. While the cystoviruses package their three ssRNA segments into preformed procapsids, the eucaryotic dsRNA viruses form their capsids around preassembled particles containing the 9–12 ssRNA segments within organized cellular structures called viral factories or viroplasm [3]. How these particles come together is complex and still requires intensive study [71].

While the dsRNA in $\Phi 6$ is arranged in ordered shells (Figure 8B), P2 and P7 are apparently not in detectable locations [35,47]. This contrasts with the cytoviruses where 10 transcriptional enzyme complexes, each composed of a polymerase and a packaging NTPase, locate to specific sites [69,70]. Somehow, during $\Phi 6$ transcription inside the nucleocapsid, P2 should be positioned at a five-fold vertex to allow a newly synthesized ssRNA transcript to be ejected by P4 on the outside. In bacteriophage $\Phi 12$, P4 acts as a passive conduit for the new transcripts [72]. Also, in $\Phi 12$, a density that could be P2 was shown underneath the five-fold vertices in virions [62]. Since there are only three segments, conceptually requiring up to three polymerases, they may not be distributed in regular locations conducive to the extensive averaging in cryoEM reconstruction.

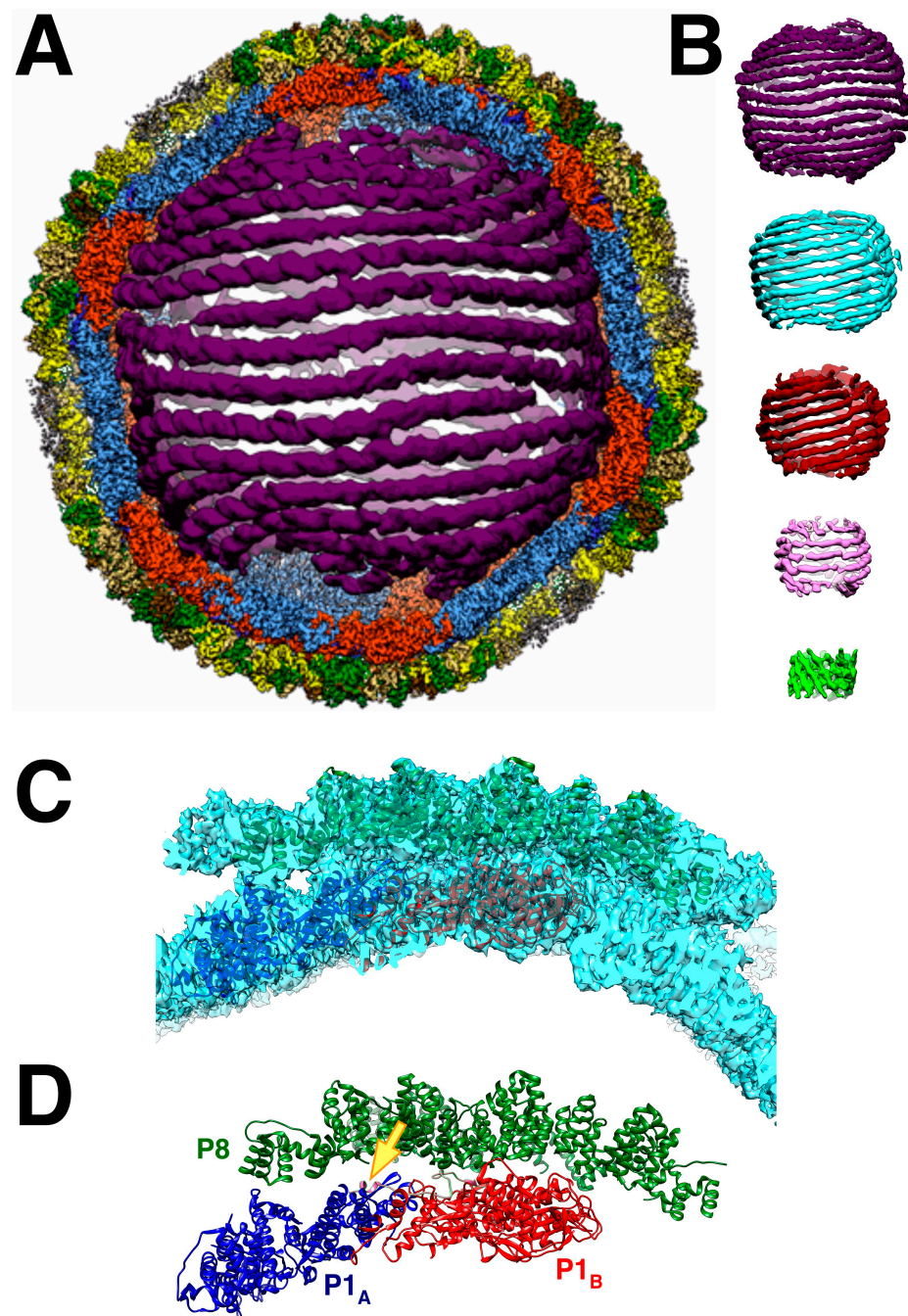


Figure 8. (A) The nucleocapsid orientated down a two-fold axis, showing a cut through the outer two layers and the first shell of dsRNA. The outer shell is the P4-P8 layer, but in this cut view, only the P8 layer is visible (green). The capsid shell is composed of the P1_A (blue) and P1_B (red) proteins. (B) The five dsRNA shells. (C) Two P1 subunits and 10 P8 monomers fitted into a reconstruction of the nucleocapsid. (D) As in C but without the density. The arrow points to the P4 C-terminal tail (pink) bound to the two P1 subunits [68].

5.2. The Intermediate Layer Composed of P4 and P8

The P8 layer is composed of 200 trimers arranged in a $T = 13$ *laevo* quasi-symmetric lattice with openings at the five-fold vertices to accommodate the P4 hexamers (Figure 8C,D) [48]. The interactions between the trimers show complicated domain-swapping features.

The P4 occupancy in the nucleocapsid is close to stoichiometric [43,68], indicating that it is assembled as such in the procapsid. The observation of lower amounts on purified

procapsids should, therefore, be considered an artifact of purification. The $\Phi 8$ P4 hexamer is offset by 8 Å from the five-fold axis of the P1 shell [44], likely the result of the symmetry mismatch with only up to five of the six C-terminal tails binding it to the P1 shell [48].

The assembly of the 16 kDa P8 protein onto the nucleocapsid requires calcium (II) Ca^{2+} , and it can be stripped off by removing Ca^{2+} [14]. Purified P8 can also self-assemble into spherical shells in the presence of Ca^{2+} , but mostly without closing [14,73]. The location where Ca^{2+} binds is not known. The assembled nucleocapsid with P8 is infective in cells where the outer membrane and peptidoglycan layers have been disrupted [14]. P8 binds to host phospholipids [74], indicating a mechanism for enveloping newly formed nucleocapsids. During infection, P8 interacts with the cell membrane to form invaginations around the nucleocapsid [75]. The nucleocapsid coated with P8 has significantly lower polymerase activity compared to the procapsid [14], such that its uncoating and degradation promote transcription [75].

5.3. The Envelope

The envelope of $\Phi 6$ is the least studied structurally because it does not conform to the icosahedral symmetry of the inner two layers. It is composed of host lipids [76] and the proteins P3, P5, P6, P9, and P10 [77,78] (Figure 1) and requires P12 for proper formation [21]. P5, the lysozyme of $\Phi 6$, is thought to be located between the envelope and the P4–P8 shell [79]. P9 is the major integral membrane protein, accompanied by P6 and P10 [79,80]. In *E. coli*, P9 expression leads to the formation of P9-containing vesicles, with P12 playing a protective role in preventing the proteolytic degradation of P9 [81]. The most prominent feature of the envelope is the mushroom-like spikes protruding from the surface, identified as P3 and anchored to the membrane by P6 [82]. The equivalent multichain P3 of $\Phi 12$ is a hexameric spike (Figure 1) [17].

6. Coopting the Host Factor YajQ for Transcription Regulation

After breaching the bacterial envelope of its host and losing the P8 layer, the $\Phi 6$ nucleocapsid transcribes its genome to produce the three ssRNA segments [83]. It was noticed that nucleocapsids produced in vitro also show suppressed expression of the L segment, unless manganese was included [84–86]. The l segment differs from the s and m segments in the second nucleotide: it is 5'-GU rather than 5'-GG. This renders the nucleocapsid unable to transcribe the l segment or any segment starting with anything other than 5'-GG [9,58]. Mn^{2+} at 1 mM overrules this blockage by increasing the permissivity of the polymerase [9,54,55]. Mn^{2+} competes with Mg^{2+} at the non-catalytic metal ion binding site in the polymerase [57]. However, the concentrations of Mn^{2+} in the host do not reach the levels required for activating the polymerase, indicating that it is not the factor stimulating l segment transcription.

Qiao et al. [15] discovered that the nucleocapsid binds an 18 kDa host protein, YajQ, required for full transcription of the L segment. A similar regulation mechanism for L transcription was described for another cystovirus, $\Phi 2954$, except that it requires a different host protein, GrxC [87]. YajQ homologues are ubiquitous and conserved in bacteria [88]. A YajQ-GFP fusion protein coated infecting $\Phi 6$ nucleocapsids to such an extent that the individual particles were visible inside cells [89]. Later in infection when many new nucleocapsids are produced, the supply of YajQ is insufficient, yielding fewer l transcripts. This is interpreted as a fortuitous regulatory function to divert resources to the other segments during final virion assembly. YajQ binds to the outside surface of the nucleocapsids and dissociates in higher salt concentration [15]. Because YajQ does not activate the polymerase directly [58], it must act through the capsid shell with the polymerase on the inside.

Purified nucleocapsids decorated with YajQ (Figure 9A) were visualized by cryoEM (Figure 9B) [90]. The micrographs show many filled capsids, but also empty P1 shells likely derived from packaged capsids that lost their RNA content (Figure 9B) [45]. YajQ binds as a monomer to 60 sites close to the three-fold axes of the icosahedral P1 shell, in this case with

an occupancy of ~58% (35 out of 60 sites) (Figure 9C). A homology model of YajQ based on the crystal structure from *Haemophilus influenzae* [91] fits unambiguously into the 3D reconstruction, indicating conservation of the fold (Figure 9D). The YajQ structure features two topologically similar domains connected by two linkers. Each domain has a beta sheet on one side and two alpha helices on the other. Each YajQ molecule straddles the two P1 subunits in the asymmetric unit, covering part of the C-terminal tail of P4 (purple density in Figure 9D).

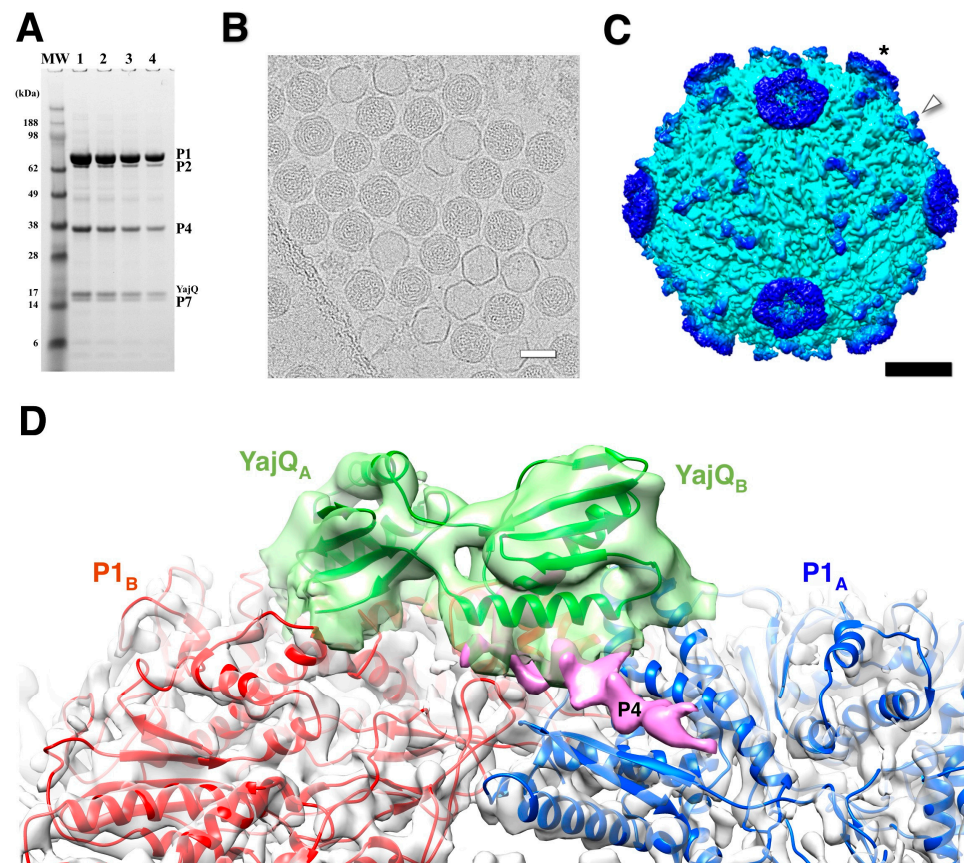


Figure 9. The bacteriophage $\Phi 6$ nucleocapsid with bound YajQ. (A) SDS-PAGE gel showing the four constituent proteins together with YajQ at a slightly larger amount than P7. (B) A representative micrograph of YajQ-bound packaged capsids with a few empty P1 shells. Scale bar: 500 Å. (C) A reconstruction of the nucleocapsid filtered to 6 Å. The YajQ monomers (arrowhead) are bound to sites surrounding the three-fold vertices. The P4 hexamers (asterisk) are the donut densities suspended above the five-fold vertices. Scale bar: 100 Å. (D) Fit of a homology model of YajQ (green) into the density attached to the capsid. Also shown are the two capsid subunits, P1_A (blue) and P1_B (red), and a purple density consistent with the C-terminal tail of P4 [90].

Purified polymerase still shows discrimination against the I segment [24], but YajQ has no effect on it [58]. The evidence points to the stability of the C-terminal domain and its role in the self-priming initiation of transcription. Manganese relieves the requirement of the $\Phi 6$ nucleocapsids for YajQ, decreasing template specificity [58]. Substitutions in two of the genes confer YajQ independence: I632V in P1, and K34N and I642V in P2 [15]. Other substitutions in the hinge region of the C-terminal domain (V603A, A604E, and L612R) increase activity in nucleocapsids in the absence of YajQ, presumably by destabilizing this domain [58].

An additional density was noted close to where YajQ binds (Figure 8D) [90] that turns out to be the C-terminal tail of P4 first described by Sun et al. [48]. This may suggest a way of action. YajQ may stabilize the tail of P4 to such an extent that it affects the expression

of the I segment. If so, the slight change at the 5' end of the I transcript may pose a higher barrier for transcription.

7. Broader Impact of the Studies on the Structure and Transformations of Bacteriophage $\Phi 6$

We have made significant progress in understanding the $\Phi 6$ life cycle, but much remains to be discovered. This relatively simple system provided some answers about dsRNA viruses, and the structural studies benefitted from recent technological advances, contributing to the development of new experimental approaches.

An important question is how a virus with a segmented genome ensures that a full complement is present in the assembled virion. Many RNA viruses with segmented genomes can package them effectively to ensure all segments are accounted for to produce an infectious particle [3,92]. In $\Phi 6$, this is achieved by the controlled sequential packaging of the three segments [93], resulting in highly structured genome packing (Figure 8A,B). This is reminiscent of the packaging in dsDNA bacteriophages into a preformed head [94]. In contrast, the current model for the packaging of eukaryotic dsRNA viruses is a coalescence of the segments into a nucleoprotein particle that is then wrapped into a capsid shell in the reoviruses [3,92] or encased in a lipid envelope in the influenza virus [95]. In all cases, packaging signals in the form of RNA structural motifs direct the proper packaging process [93,96].

Many icosahedral virus capsids can self-assemble, often with the help of scaffolding partners [97,98]. In $\Phi 6$, the scaffolding role for P1 assembly is assumed mainly by P4, with assistance from P2 and P7 [19,59,60]. As with many procapsids, it assembles in a metastable state that can transform into a more stable mature form in $\Phi 6$, concurrent with packaging and expansion (Figure 7).

The studies of the $\Phi 6$ procapsid and nucleocapsid structures grew with the development of better capabilities in electron microscopes as well as computational approaches to processing micrographs. The discovery of the locations of the P2 and P7 proteins was directly related to better reconstruction of cryoEM maps and examining difference maps between procapsids with different compositions [32,34,35]. Knowing these locations, we could count the presence of the molecules using cryo-electron tomography and obtain detailed distributions of occupancy [33]. New techniques to handle symmetry mismatch were developed for understanding the structures of P4, P2, and dsRNA within the context of the procapsid and nucleocapsid [47,48,68]. We combined X-ray crystallography of the P1 pentamer with the high-resolution cryoEM maps of the procapsid and nucleocapsid to visualize the conformational differences between subunits and the transformations during capsid expansion [37]. We now have tools to study viruses in great structural detail, so the success of a project is largely determined by the quality of sample preparation.

The remarkable progress in structural biology has given us a detailed understanding of the dsRNA and two inner layers of the $\Phi 6$ virion and its transformations during its life cycle. Nevertheless, there are many questions that remain to be answered. The full sequence of events in procapsid assembly would contribute to resolving how complete icosahedral particles form. How do the three ssRNA segments recognize the conformational state of the procapsid? How is the nucleocapsid enveloped in the final stages of virion formation? The detailed structures of the integral proteins in the envelope and the spike still need to be determined. What triggers the lysis of the host cell? Structural details of the infection events are required to better understand how it binds to pili and breaches the cell envelope. After infection, is the P4 hexamer involved in the transmission of control from YajQ to the polymerase inside the P1 shell? There is ample room for further structural studies of the cystoviruses for their own sake but also in the broader context of protein interactions and dynamics, and not only pertinent to viruses.

Funding: This project was funded using Federal funds from the Frederick National Laboratory for Cancer Research, National Institutes of Health (contract No. HHSN75N91019D00024).

Data Availability Statement: All structural data used in preparing the review can be found in the Electron Microscopy Databank (<https://www.ebi.ac.uk/emdb>, accessed on 23 October 2023) and the Protein Data Bank (<https://www.rcsb.org>, accessed on 23 October 2023).

Conflicts of Interest: Author J Bernard Heymann was employed by the company Leidos Biomedical Research, Inc. The author declares that the research was conducted in the absence of any commercial or financial relationships that could be construed as a potential conflict of interest. The funders had no role in the design of the study; in the collection, analyses, or interpretation of data; in the writing of the manuscript; or in the decision to publish the results.

References

1. Vidaver, A.K.; Koski, R.K.; Van Etten, J.L. Bacteriophage $\phi 6$: A Lipid-Containing Virus of *Pseudomonas phaseolicola*. *J. Virol.* **1973**, *11*, 799–805. [[CrossRef](#)] [[PubMed](#)]
2. Mantynen, S.; Sundberg, L.R.; Poranen, M.M. Recognition of six additional cystoviruses: *Pseudomonas virus* $\phi 6$ is no longer the sole species of the family Cystoviridae. *Arch. Virol.* **2018**, *163*, 1117–1124. [[CrossRef](#)] [[PubMed](#)]
3. Borodavka, A.; Desselberger, U.; Patton, J.T. Genome packaging in multi-segmented dsRNA viruses: Distinct mechanisms with similar outcomes. *Curr. Opin. Virol.* **2018**, *33*, 106–112. [[CrossRef](#)] [[PubMed](#)]
4. Serrano-Aroca, A. Antiviral Characterization of Advanced Materials: Use of Bacteriophage Phi 6 as Surrogate of Enveloped Viruses Such as SARS-CoV-2. *Int. J. Mol. Sci.* **2022**, *23*, 5335. [[CrossRef](#)]
5. Chen, Y.G.; Hur, S. Cellular origins of dsRNA, their recognition and consequences. *Nat. Rev. Mol. Cell Biol.* **2022**, *23*, 286–301. [[CrossRef](#)]
6. Pinheiro, L.A.M.; Pereira, C.; Barreal, M.E.; Gallego, P.P.; Balcao, V.M.; Almeida, A. Use of phage $\phi 6$ to inactivate *Pseudomonas syringae* pv. *actinidiae* in kiwifruit plants: In Vitro and ex vivo experiments. *Appl. Microbiol. Biotechnol.* **2020**, *104*, 1319–1330. [[CrossRef](#)]
7. Pinheiro, L.A.M.; Pereira, C.; Frazao, C.; Balcao, V.M.; Almeida, A. Efficiency of Phage $\phi 6$ for Biocontrol of *Pseudomonas syringae* pv. *syringae*: An in Vitro Preliminary Study. *Microorganisms* **2019**, *7*, 286. [[CrossRef](#)]
8. de Carvalho, N.A.; Stachler, E.N.; Cimabue, N.; Bibby, K. Evaluation of $\Phi 6$ Persistence and Suitability as an Enveloped Virus Surrogate. *Environ. Sci. Technol.* **2017**, *51*, 8692–8700. [[CrossRef](#)]
9. Frilander, M.; Poranen, M.; Bamford, D.H. The large genome segment of dsRNA bacteriophage $\phi 6$ is the key regulator in the in vitro minus and plus strand synthesis. *RNA* **1995**, *1*, 510–518.
10. Cuppels, D.A.; Van Etten, J.L.; Burbank, D.E.; Lane, L.C.; Vidaver, A.K. In vitro translation of the three bacteriophage $\phi 6$ RNAs. *J. Virol.* **1980**, *35*, 249–251. [[CrossRef](#)]
11. Bamford, D.H.; Romantschuk, M.; Somerharju, P.J. Membrane fusion in prokaryotes: Bacteriophage $\phi 6$ membrane fuses with the *Pseudomonas syringae* outer membrane. *EMBO J.* **1987**, *6*, 1467–1473. [[CrossRef](#)] [[PubMed](#)]
12. Mindich, L.; Lehman, J. Cell wall lysin as a component of the bacteriophage $\phi 6$ virion. *J. Virol.* **1979**, *30*, 489–496. [[CrossRef](#)]
13. Caldentey, J.; Bamford, D.H. The lytic enzyme of the *Pseudomonas* phage $\phi 6$: Purification and biochemical characterization. *Biochim. Biophys. Acta* **1992**, *1159*, 44–50. [[CrossRef](#)] [[PubMed](#)]
14. Olkkonen, V.M.; Ojala, P.M.; Bamford, D.H. Generation of infectious nucleocapsids by in vitro assembly of the shell protein on to the polymerase complex of the dsRNA bacteriophage $\phi 6$. *J. Mol. Biol.* **1991**, *218*, 569–581. [[CrossRef](#)] [[PubMed](#)]
15. Qiao, X.; Sun, Y.; Qiao, J.; Mindich, L. The role of host protein YajQ in the temporal control of transcription in bacteriophage $\Phi 6$. *Proc. Natl. Acad. Sci. USA* **2008**, *105*, 15956–15960. [[CrossRef](#)] [[PubMed](#)]
16. Jaalinoja, H.T.; Huiskonen, J.T.; Butcher, S.J. Electron cryomicroscopy comparison of the architectures of the enveloped bacteriophages $\phi 6$ and $\phi 8$. *Structure* **2007**, *15*, 157–167. [[CrossRef](#)] [[PubMed](#)]
17. Leo-Macias, A.; Katz, G.; Wei, H.; Alimova, A.; Katz, A.; Rice, W.J.; Diaz-Avalos, R.; Hu, G.B.; Stokes, D.L.; Gottlieb, P. Toroidal surface complexes of bacteriophage $\phi 12$ are responsible for host-cell attachment. *Virology* **2011**, *414*, 103–109. [[CrossRef](#)] [[PubMed](#)]
18. Mindich, L.; Davidoff-Abelson, R. The characterization of a 120 S particle formed during $\phi 6$ infection. *Virology* **1980**, *103*, 386–391. [[CrossRef](#)]
19. Gottlieb, P.; Strassman, J.; Bamford, D.H.; Mindich, L. Production of a polyhedral particle in *Escherichia coli* from a cDNA copy of the large genomic segment of bacteriophage $\phi 6$. *J. Virol.* **1988**, *62*, 181–187. [[CrossRef](#)]
20. Qiao, X.; Casini, G.; Qiao, J.; Mindich, L. In vitro packaging of individual genomic segments of bacteriophage $\phi 6$ RNA: Serial dependence relationships. *J. Virol.* **1995**, *69*, 2926–2931. [[CrossRef](#)]
21. Johnson, M.D., 3rd; Mindich, L. Plasmid-directed assembly of the lipid-containing membrane of bacteriophage $\phi 6$. *J. Bacteriol.* **1994**, *176*, 4124–4132. [[CrossRef](#)] [[PubMed](#)]
22. Johnson, M.D., 3rd; Mindich, L. Isolation and characterization of nonsense mutations in gene 10 of bacteriophage $\phi 6$. *J. Virol.* **1994**, *68*, 2331–2338. [[CrossRef](#)] [[PubMed](#)]
23. Day, L.A.; Mindich, L. The molecular weight of bacteriophage $\phi 6$ and its nucleocapsid. *Virology* **1980**, *103*, 376–385. [[CrossRef](#)] [[PubMed](#)]

24. Makeyev, E.V.; Bamford, D.H. Replicase activity of purified recombinant protein P2 of double-stranded RNA bacteriophage $\phi 6$. *EMBO J.* **2000**, *19*, 124–133. [[CrossRef](#)] [[PubMed](#)]
25. Gottlieb, P.; Strassman, J.; Mindich, L. Protein P4 of the bacteriophage $\phi 6$ procapsid has a nucleoside triphosphate-binding site with associated nucleoside triphosphate phosphohydrolase activity. *J. Virol.* **1992**, *66*, 6220–6222. [[CrossRef](#)] [[PubMed](#)]
26. Paatero, A.O.; Syvaioja, J.E.; Bamford, D.H. Double-stranded RNA bacteriophage $\phi 6$ protein P4 is an unspecific nucleoside triphosphatase activated by calcium ions. *J. Virol.* **1995**, *69*, 6729–6734. [[CrossRef](#)] [[PubMed](#)]
27. Juuti, J.T.; Bamford, D.H. RNA binding, packaging and polymerase activities of the different incomplete polymerase complex particles of dsRNA bacteriophage $\phi 6$. *J. Mol. Biol.* **1995**, *249*, 545–554. [[CrossRef](#)]
28. Juuti, J.T.; Bamford, D.H. Protein P7 of phage $\phi 6$ RNA polymerase complex, acquiring of RNA packaging activity by in vitro assembly of the purified protein onto deficient particles. *J. Mol. Biol.* **1997**, *266*, 891–900. [[CrossRef](#)]
29. Olkkonen, V.M.; Bamford, D.H. The nucleocapsid of the lipid-containing double-stranded RNA bacteriophage $\phi 6$ contains a protein skeleton consisting of a single polypeptide species. *J. Virol.* **1987**, *61*, 2362–2367. [[CrossRef](#)]
30. Butcher, S.J.; Dokland, T.; Ojala, P.M.; Bamford, D.H.; Fuller, S.D. Intermediates in the assembly pathway of the double-stranded RNA virus $\phi 6$. *EMBO J.* **1997**, *16*, 4477–4487. [[CrossRef](#)]
31. Huiskonen, J.T.; de Haas, F.; Bubeck, D.; Bamford, D.H.; Fuller, S.D.; Butcher, S.J. Structure of the bacteriophage $\phi 6$ nucleocapsid suggests a mechanism for sequential RNA packaging. *Structure* **2006**, *14*, 1039–1048. [[CrossRef](#)]
32. Sen, A.; Heymann, J.B.; Cheng, N.; Qiao, J.; Mindich, L.; Steven, A.C. Initial location of the RNA-dependent RNA polymerase in the bacteriophage $\Phi 6$ procapsid determined by cryo-electron microscopy. *J. Biol. Chem.* **2008**, *283*, 12227–12231. [[CrossRef](#)] [[PubMed](#)]
33. Nemecek, D.; Heymann, J.B.; Qiao, J.; Mindich, L.; Steven, A.C. Cryo-electron tomography of bacteriophage $\phi 6$ procapsids shows random occupancy of the binding sites for RNA polymerase and packaging NTPase. *J. Struct. Biol.* **2010**, *171*, 389–396. [[CrossRef](#)] [[PubMed](#)]
34. Katz, G.; Wei, H.; Alimova, A.; Katz, A.; Morgan, D.G.; Gottlieb, P. Protein P7 of the cystovirus $\phi 6$ is located at the three-fold axis of the unexpanded procapsid. *PLoS ONE* **2012**, *7*, e47489. [[CrossRef](#)] [[PubMed](#)]
35. Nemecek, D.; Qiao, J.; Mindich, L.; Steven, A.C.; Heymann, J.B. Packaging accessory protein P7 and polymerase P2 have mutually occluding binding sites inside the bacteriophage $\phi 6$ procapsid. *J. Virol.* **2012**, *86*, 11616–11624. [[CrossRef](#)] [[PubMed](#)]
36. Luque, D.; Mata, C.P.; Suzuki, N.; Ghabrial, S.A.; Caston, J.R. Capsid Structure of dsRNA Fungal Viruses. *Viruses* **2018**, *10*, 481. [[CrossRef](#)] [[PubMed](#)]
37. Nemecek, D.; Boura, E.; Wu, W.; Cheng, N.; Plevka, P.; Qiao, J.; Mindich, L.; Heymann, J.B.; Hurley, J.H.; Steven, A.C. Subunit folds and maturation pathway of a dsRNA virus capsid. *Structure* **2013**, *21*, 1374–1383. [[CrossRef](#)]
38. El Omari, K.; Sutton, G.; Ravantti, J.J.; Zhang, H.; Walter, T.S.; Grimes, J.M.; Bamford, D.H.; Stuart, D.I.; Mancini, E.J. Plate tectonics of virus shell assembly and reorganization in phage $\phi 8$, a distant relative of mammalian reoviruses. *Structure* **2013**, *21*, 1384–1395. [[CrossRef](#)]
39. Caspar, D.L.; Klug, A. Physical principles in the construction of regular viruses. *Cold Spring Harb. Symp. Quant. Biol.* **1962**, *27*, 1–24. [[CrossRef](#)]
40. Juuti, J.T.; Bamford, D.H.; Tuma, R.; Thomas, G.J., Jr. Structure and NTPase activity of the RNA-translocating protein (P4) of bacteriophage $\phi 6$. *J. Mol. Biol.* **1998**, *279*, 347–359. [[CrossRef](#)]
41. El Omari, K.; Meier, C.; Kainov, D.; Sutton, G.; Grimes, J.M.; Poranen, M.M.; Bamford, D.H.; Tuma, R.; Stuart, D.I.; Mancini, E.J. Tracking in atomic detail the functional specializations in viral RecA helicases that occur during evolution. *Nucleic Acids Res.* **2013**, *41*, 9396–9410. [[CrossRef](#)] [[PubMed](#)]
42. de Haas, F.; Paatero, A.O.; Mindich, L.; Bamford, D.H.; Fuller, S.D. A symmetry mismatch at the site of RNA packaging in the polymerase complex of dsRNA bacteriophage $\phi 6$. *J. Mol. Biol.* **1999**, *294*, 357–372. [[CrossRef](#)]
43. Sun, X.; Bamford, D.H.; Poranen, M.M. Probing, by self-assembly, the number of potential binding sites for minor protein subunits in the procapsid of double-stranded RNA bacteriophage $\Phi 6$. *J. Virol.* **2012**, *86*, 12208–12216. [[CrossRef](#)] [[PubMed](#)]
44. Huiskonen, J.T.; Jaalinoja, H.T.; Briggs, J.A.; Fuller, S.D.; Butcher, S.J. Structure of a hexameric RNA packaging motor in a viral polymerase complex. *J. Struct. Biol.* **2007**, *158*, 156–164. [[CrossRef](#)] [[PubMed](#)]
45. Nemecek, D.; Cheng, N.; Qiao, J.; Mindich, L.; Steven, A.C.; Heymann, J.B. Stepwise expansion of the bacteriophage $\phi 6$ procapsid: Possible packaging intermediates. *J. Mol. Biol.* **2011**, *414*, 260–271. [[CrossRef](#)] [[PubMed](#)]
46. Futerman, E. *$\phi 6$ Polymerase Conformation; RNA Packaging Portal Stability*; CUNY Academic Works; City College of New York, CUNY: New York, NY, USA, 2012.
47. Ilca, S.L.; Kotecha, A.; Sun, X.; Poranen, M.M.; Stuart, D.I.; Huiskonen, J.T. Localized reconstruction of subunits from electron cryomicroscopy images of macromolecular complexes. *Nat. Commun.* **2015**, *6*, 8843. [[CrossRef](#)]
48. Sun, Z.; El Omari, K.; Sun, X.; Ilca, S.L.; Kotecha, A.; Stuart, D.I.; Poranen, M.M.; Huiskonen, J.T. Double-stranded RNA virus outer shell assembly by bona fide domain-swapping. *Nat. Commun.* **2017**, *8*, 14814. [[CrossRef](#)] [[PubMed](#)]
49. Paatero, A.O.; Mindich, L.; Bamford, D.H. Mutational analysis of the role of nucleoside triphosphatase P4 in the assembly of the RNA polymerase complex of bacteriophage $\phi 6$. *J. Virol.* **1998**, *72*, 10058–10065. [[CrossRef](#)]
50. Sinclair, J.F.; Mindich, L. RNA synthesis during infection with bacteriophage $\phi 6$. *Virology* **1976**, *75*, 209–217. [[CrossRef](#)]

51. Gottlieb, P.; Strassman, J.; Qiao, X.Y.; Frucht, A.; Mindich, L. In vitro replication, packaging, and transcription of the segmented double-stranded RNA genome of bacteriophage $\phi 6$: Studies with procapsids assembled from plasmid-encoded proteins. *J. Bacteriol.* **1990**, *172*, 5774–5782. [[CrossRef](#)]
52. Butcher, S.J.; Grimes, J.M.; Makeyev, E.V.; Bamford, D.H.; Stuart, D.I. A mechanism for initiating RNA-dependent RNA polymerization. *Nature* **2001**, *410*, 235–240. [[CrossRef](#)] [[PubMed](#)]
53. Sarin, L.P.; Wright, S.; Chen, Q.; Degerth, L.H.; Stuart, D.I.; Grimes, J.M.; Bamford, D.H.; Poranen, M.M. The C-terminal priming domain is strongly associated with the main body of bacteriophage $\phi 6$ RNA-dependent RNA polymerase. *Virology* **2012**, *432*, 184–193. [[CrossRef](#)] [[PubMed](#)]
54. Poranen, M.M.; Koivunen, M.R.; Bamford, D.H. Nontemplated terminal nucleotidyltransferase activity of double-stranded RNA bacteriophage $\phi 6$ RNA-dependent RNA polymerase. *J. Virol.* **2008**, *82*, 9254–9264. [[CrossRef](#)] [[PubMed](#)]
55. Poranen, M.M.; Salgado, P.S.; Koivunen, M.R.; Wright, S.; Bamford, D.H.; Stuart, D.I.; Grimes, J.M. Structural explanation for the role of Mn²⁺ in the activity of $\phi 6$ RNA-dependent RNA polymerase. *Nucleic Acids Res.* **2008**, *36*, 6633–6644. [[CrossRef](#)]
56. Yang, H.; Makeyev, E.V.; Bamford, D.H. Comparison of polymerase subunits from double-stranded RNA bacteriophages. *J. Virol.* **2001**, *75*, 11088–11095. [[CrossRef](#)]
57. Wright, S.; Poranen, M.M.; Bamford, D.H.; Stuart, D.I.; Grimes, J.M. Noncatalytic ions direct the RNA-dependent RNA polymerase of bacterial double-stranded RNA virus $\phi 6$ from de novo initiation to elongation. *J. Virol.* **2012**, *86*, 2837–2849. [[CrossRef](#)]
58. Qiao, J.; Mindich, L. The template specificity of bacteriophage $\Phi 6$ RNA polymerase. *J. Virol.* **2013**, *87*, 10190–10194. [[CrossRef](#)]
59. Sun, X.; Ilca, S.L.; Huiskonen, J.T.; Poranen, M.M. Dual Role of a Viral Polymerase in Viral Genome Replication and Particle Self-Assembly. *mBio* **2018**, *9*, e01242-18. [[CrossRef](#)]
60. Poranen, M.M.; Paatero, A.O.; Tuma, R.; Bamford, D.H. Self-assembly of a viral molecular machine from purified protein and RNA constituents. *Mol. Cell* **2001**, *7*, 845–854. [[CrossRef](#)]
61. Eryilmaz, E.; Benach, J.; Su, M.; Seetharaman, J.; Dutta, K.; Wei, H.; Gottlieb, P.; Hunt, J.F.; Ghose, R. Structure and dynamics of the P7 protein from the bacteriophage $\phi 12$. *J. Mol. Biol.* **2008**, *382*, 402–422. [[CrossRef](#)]
62. Wei, H.; Cheng, R.H.; Berriman, J.; Rice, W.J.; Stokes, D.L.; Katz, A.; Morgan, D.G.; Gottlieb, P. Three-dimensional structure of the enveloped bacteriophage $\phi 12$: An incomplete T = 13 lattice is superposed on an enclosed T = 1 shell. *PLoS ONE* **2009**, *4*, e6850. [[CrossRef](#)] [[PubMed](#)]
63. Ikonen, T.; Kainov, D.; Timmins, P.; Serimaa, R.; Tuma, R. Locating the minor components of double-stranded RNA bacteriophage 6 by neutron scattering. *J. Appl. Crystall.* **2003**, *36*, 525–529. [[CrossRef](#)]
64. Dokland, T. Scaffolding proteins and their role in viral assembly. *Cell Mol. Life Sci.* **1999**, *56*, 580–603. [[CrossRef](#)] [[PubMed](#)]
65. Trask, S.D.; McDonald, S.M.; Patton, J.T. Structural insights into the coupling of virion assembly and rotavirus replication. *Nat. Rev. Microbiol.* **2012**, *10*, 165–177. [[CrossRef](#)]
66. Frilander, M.; Bamford, D.H. In Vitro packaging of the single-stranded RNA genomic precursors of the segmented double-stranded RNA bacteriophage $\phi 6$: The three segments modulate each other's packaging efficiency. *J. Mol. Biol.* **1995**, *246*, 418–428. [[CrossRef](#)]
67. Pirttimaa, M.J.; Paatero, A.O.; Frilander, M.J.; Bamford, D.H. Nonspecific nucleoside triphosphatase P4 of double-stranded RNA bacteriophage $\phi 6$ is required for single-stranded RNA packaging and transcription. *J. Virol.* **2002**, *76*, 10122–10127. [[CrossRef](#)]
68. Ilca, S.L.; Sun, X.; El Omari, K.; Kotecha, A.; de Haas, F.; DiMaio, F.; Grimes, J.M.; Stuart, D.I.; Poranen, M.M.; Huiskonen, J.T. Multiple liquid crystalline geometries of highly compacted nucleic acid in a dsRNA virus. *Nature* **2019**, *570*, 252–256. [[CrossRef](#)]
69. Liu, H.; Cheng, L. Cryo-EM shows the polymerase structures and a nonspooled genome within a dsRNA virus. *Science* **2015**, *349*, 1347–1350. [[CrossRef](#)]
70. Zhang, X.; Ding, K.; Yu, X.; Chang, W.; Sun, J.; Zhou, Z.H. In situ structures of the segmented genome and RNA polymerase complex inside a dsRNA virus. *Nature* **2015**, *527*, 531–534. [[CrossRef](#)]
71. Strauss, S.; Acker, J.; Papa, G.; Desiro, D.; Schueder, F.; Borodavka, A.; Jungmann, R. Principles of RNA recruitment to viral ribonucleoprotein condensates in a segmented dsRNA virus. *eLife* **2023**, *12*, e68670. [[CrossRef](#)]
72. Kainov, D.E.; Lisal, J.; Bamford, D.H.; Tuma, R. Packaging motor from double-stranded RNA bacteriophage $\phi 12$ acts as an obligatory passive conduit during transcription. *Nucleic Acids Res.* **2004**, *32*, 3515–3521. [[CrossRef](#)] [[PubMed](#)]
73. Tuma, R.; Bamford, J.K.; Bamford, D.H.; Thomas, G.J., Jr. Assembly dynamics of the nucleocapsid shell subunit (P8) of bacteriophage $\phi 6$. *Biochemistry* **1999**, *38*, 15025–15033. [[CrossRef](#)] [[PubMed](#)]
74. Cvirkaite-Krupovic, V.; Poranen, M.M.; Bamford, D.H. Phospholipids act as secondary receptor during the entry of the enveloped, double-stranded RNA bacteriophage $\phi 6$. *J. Gen. Virol.* **2010**, *91*, 2116–2120. [[CrossRef](#)] [[PubMed](#)]
75. Romantschuk, M.; Olkkonen, V.M.; Bamford, D.H. The nucleocapsid of bacteriophage $\phi 6$ penetrates the host cytoplasmic membrane. *EMBO J.* **1988**, *7*, 1821–1829. [[CrossRef](#)] [[PubMed](#)]
76. Laurinavicius, S.; Kakela, R.; Bamford, D.H.; Somerharju, P. The origin of phospholipids of the enveloped bacteriophage $\phi 6$. *Virology* **2004**, *326*, 182–190. [[CrossRef](#)] [[PubMed](#)]
77. Sinclair, J.F.; Tzagoloff, A.; Levine, D.; Mindich, L. Proteins of bacteriophage $\phi 6$. *J. Virol.* **1975**, *16*, 685–695. [[CrossRef](#)] [[PubMed](#)]
78. Van Etten, J.; Lane, L.; Gonzalez, C.; Partridge, J.; Vidaver, A. Comparative properties of bacteriophage $\phi i 6$ and $\phi i 6$ nucleocapsid. *J. Virol.* **1976**, *18*, 652–658. [[CrossRef](#)]
79. Stitt, B.L.; Mindich, L. The structure of bacteriophage $\phi 6$: Protease digestion of $\phi 6$ virions. *Virology* **1983**, *127*, 459–462. [[CrossRef](#)]

80. Stitt, B.L.; Mindich, L. Morphogenesis of bacteriophage $\phi 6$: A presumptive viral membrane precursor. *Virology* **1983**, *127*, 446–458. [[CrossRef](#)]
81. Lyytinen, O.L.; Starkova, D.; Poranen, M.M. Microbial production of lipid-protein vesicles using enveloped bacteriophage $\phi 6$. *Microb. Cell Fact.* **2019**, *18*, 29. [[CrossRef](#)]
82. Kenney, J.M.; Hantula, J.; Fuller, S.D.; Mindich, L.; Ojala, P.M.; Bamford, D.H. Bacteriophage $\phi 6$ envelope elucidated by chemical cross-linking, immunodetection, and cryoelectron microscopy. *Virology* **1992**, *190*, 635–644. [[CrossRef](#)] [[PubMed](#)]
83. Emori, Y.; Iba, H.; Okada, Y. Semi-conservative transcription of double-stranded RNA catalyzed by bacteriophage $\phi 6$ RNA polymerase. *J. Biochem.* **1980**, *88*, 1569–1575. [[CrossRef](#)] [[PubMed](#)]
84. Coplin, D.L.; Van Etten, J.L.; Koski, R.K.; Vidaver, A.K. Intermediates in the biosynthesis of double-stranded ribonucleic acids of bacteriophage $\phi 6$. *Proc. Natl. Acad. Sci. USA* **1975**, *72*, 849–853. [[CrossRef](#)] [[PubMed](#)]
85. Emori, Y.; Iba, H.; Okada, Y. Transcriptional regulation of three double-stranded RNA segments of bacteriophage phi 6 in vitro. *J. Virol.* **1983**, *46*, 196–203. [[CrossRef](#)] [[PubMed](#)]
86. Ojala, P.M.; Bamford, D.H. In vitro transcription of the double-stranded RNA bacteriophage $\phi 6$ is influenced by purine NTPs and calcium. *Virology* **1995**, *207*, 400–408. [[CrossRef](#)] [[PubMed](#)]
87. Qiao, J.; Qiao, X.; Sun, Y.; Mindich, L. Role of host protein glutaredoxin 3 in the control of transcription during bacteriophage $\phi 2954$ infection. *Proc. Natl. Acad. Sci. USA* **2010**, *107*, 6000–6004. [[CrossRef](#)] [[PubMed](#)]
88. Miron, S.; Borza, T.; Saveanu, C.; Gilles, A.M.; Barzu, O.; Craescu, C.T. ¹H, ¹³C and ¹⁵N resonance assignment of YajQ, a protein of unknown structure and function from Escherichia coli. *J. Biomol. NMR* **2001**, *20*, 287–288. [[CrossRef](#)] [[PubMed](#)]
89. Qiao, X.; Sun, Y.; Qiao, J.; Mindich, L. Interaction of a host protein with core complexes of bacteriophage $\phi 6$ to control transcription. *J. Virol.* **2010**, *84*, 4821–4825. [[CrossRef](#)]
90. Heymann, J.B.; Nemecek, D.; Huang, R.; Cheng, N.; Qiao, J.; Mindich, L.; Steven, A.C. A Polymerase-Activating Host Factor, YajQ, Bound to the Bacteriophage $\phi 6$ Capsid. *Microsc. Microanal.* **2016**, *22*, 1110–1111. [[CrossRef](#)]
91. Teplyakov, A.; Obmolova, G.; Bir, N.; Reddy, P.; Howard, A.J.; Gilliland, G.L. Crystal structure of the YajQ protein from Haemophilus influenzae reveals a tandem of RNP-like domains. *J. Struct. Funct. Genomics* **2003**, *4*, 1–9. [[CrossRef](#)]
92. McDonald, S.M.; Nelson, M.I.; Turner, P.E.; Patton, J.T. Reassortment in segmented RNA viruses: Mechanisms and outcomes. *Nat. Rev. Microbiol.* **2016**, *14*, 448–460. [[CrossRef](#)] [[PubMed](#)]
93. Mindich, L. Precise packaging of the three genomic segments of the double-stranded-RNA bacteriophage $\phi 6$. *Microbiol. Mol. Biol. Rev.* **1999**, *63*, 149–160. [[CrossRef](#)] [[PubMed](#)]
94. Rao, V.B.; Feiss, M. Mechanisms of DNA Packaging by Large Double-Stranded DNA Viruses. *Annu. Rev. Virol.* **2015**, *2*, 351–378. [[CrossRef](#)] [[PubMed](#)]
95. Haralampiev, I.; Prisner, S.; Nitzan, M.; Schade, M.; Jolmes, F.; Schreiber, M.; Loidolt-Kruger, M.; Jongen, K.; Chamiolo, J.; Nilson, N.; et al. Selective flexible packaging pathways of the segmented genome of influenza A virus. *Nat. Commun.* **2020**, *11*, 4355. [[CrossRef](#)] [[PubMed](#)]
96. Ye, L.; Ambi, U.B.; Olguin-Nava, M.; Gribling-Burrer, A.S.; Ahmad, S.; Bohn, P.; Weber, M.M.; Smyth, R.P. RNA Structures and Their Role in Selective Genome Packaging. *Viruses* **2021**, *13*, 1788. [[CrossRef](#)]
97. Selivanovitch, E.; Douglas, T. Virus capsid assembly across different length scales inspire the development of virus-based biomaterials. *Curr. Opin. Virol.* **2019**, *36*, 38–46. [[CrossRef](#)]
98. Perlmutter, J.D.; Hagan, M.F. Mechanisms of virus assembly. *Annu. Rev. Phys. Chem.* **2015**, *66*, 217–239. [[CrossRef](#)]

Disclaimer/Publisher’s Note: The statements, opinions and data contained in all publications are solely those of the individual author(s) and contributor(s) and not of MDPI and/or the editor(s). MDPI and/or the editor(s) disclaim responsibility for any injury to people or property resulting from any ideas, methods, instructions or products referred to in the content.